Preprints.org

Article

Not peer-reviewed version

Optimization of Processing Parameters and Application Performance Evaluation of a High Thermal Conductivity, Low Thermal Resistance Gel

Yuwen Xu * , Danni Hong , Liangjun Liu , Wenfei Wang , Minghua Jiang , Haibing Yang , Tingxin Chen , Kun Jia

Posted Date: 2 March 2026

doi: 10.20944/preprints202603.0106.v1

Keywords: thermal interface materials; thermal conductive gel; interfacical thermal resistance; filler ratio; wetting time; silicone oil viscosity

Preprints.org is a free multidisciplinary platform providing preprint service that is dedicated to making early versions of research outputs permanently available and citable. Preprints posted at Preprints.org appear in Web of Science, Crossref, Google Scholar, Scilit, Europe PMC.

Copyright: This open access article is published under a Creative Commons CC BY 4.0 license, which permit the free download, distribution, and reuse, provided that the author and preprint are cited in any reuse.

Preprints.org (www.preprints.org) | NOT PEER-REVIEWED | Posted: 2 March 2026 doi:10.20944/preprints202603.0106.v1

Disclaimer/Publisher's Note: The statements, opinions, and data contained in all publications are solely those of the individual author(s) and contributor(s) and not of MDPI and/or the editor(s). MDPI and/or the editor(s) disclaim responsibility for any injury to people or property resulting from any ideas, methods, instructions, or products referred to in the content.

Article

Optimization of Processing Parameters and Application Performance Evaluation of a High Thermal Conductivity, Low Thermal Resistance Gel

Yuwen Xu [1,*], Danni Hong [2], Liangjun Liu [3], Wenfei Wang [3], Minghua Jiang [3], Haibing Yang [3], Tingxin Chen [1] and Kun Jia [4]

1 South China University of Technology
2 China Science and Technology on Reliability Physics and Application of Electronic Component Laboratory, Guangzhou
3 U-Bond Mater. Tech. Inc., Dongguan China
4 University of Electronic Science and Technology of China
* Correspondence: xyw_ubond@163.com

Abstract

Thermal interface materials (TIMs) are essential for addressing heat dissipation challenges in high-performance electronic devices. Among various TIMs, thermal conductive gels exhibit significant potential in high heat flux applications due to their excellent flexibility and superior gap-filling capability. Current research primarily concentrates on the fabrication and performance characterization of novel thermal conductive gels, while comparatively little attention has been devoted to the optimization of processing parameters. Furthermore, existing characterization methods often fail to accurately replicate real-world operating conditions, resulting in discrepancies between laboratory measurements and actual performance. An orthogonal experimental design was adopted to systematically elucidate the influence of filler ratio, wetting time, and silicone oil viscosity on the bonding strength of thermal conductive gels. The filler ratio exerts the most significant influence, followed by silicone oil viscosity and wetting time. Subsequently, the thermal conductivity and thermal resistance of both commercial thermal conductive gels and the as-prepared gels were characterized using the steady-state heat flow method and the double-interface method, respectively. The prepared thermal conductive gel exhibits a thermal conductivity of 3.75 $W{\cdot}m^{-1}{\cdot}K^{-1}$ and a service thermal resistance of 0.611 $°C{\cdot}W^{-1}$, outperforming commercial counterparts and demonstrating promising application potential. This study provides a practical reference for the development and engineering application of high thermal conductivity, low thermal resistance thermal conductive gels.

Keywords: thermal interface materials; thermal conductive gel; interfacical thermal resistance; filler ratio; wetting time; silicone oil viscosity

1. Introduction

With the continuous advancement of electronic components toward higher power density, miniaturization, and greater integration, heat flux density has increased significantly, rendering thermal management of chips an increasingly critical challenge [1–3]. In practical applications, the actual contact area between a chip and a heat sink accounts for only approximately 10% of the apparent macroscopic contact area, while the remaining interfacial region is filled with air, which exhibits an extremely low thermal conductivity of only 0.03 $W{\cdot}m^{-1}{\cdot}K^{-1}$[4–6]. Such interfacial thermal resistance severely impedes heat dissipation efficiency. Previous studies have reported that the reliability of an electronic system may decrease by nearly 50% for every 10 °C increase in operating temperature [7,8]. Therefore, the development of high-performance thermal interface materials (TIMs) for high-power chips has become a prominent research focus. TIMs primarily include thermal

© 2026 by the author(s). Distributed under a Creative Commons CC BY license.

Preprints.org (www.preprints.org) | NOT PEER-REVIEWED | Posted: 2 March 2026 doi:10.20944/preprints202603.0106.v1

conductive pads, thermal conductive silicone grease, and thermal conductive gels. Among these, thermal conductive silicone grease often suffers from structural instability during long-term operation due to the oil-pumping effect [9]. In contrast, the relatively large thickness and high elastic modulus of thermal conductive pads tend to increase interfacial contact thermal resistance [10,11]. Compared with thermal conductive pads and silicone grease, thermal conductive gels exhibit unique advantages in high heat flux applications owing to their intrinsic flexibility, high thermal conductivity potential, and excellent gap-filling capability. Consequently, they demonstrate irreplaceable application value in 5G communication base stations, artificial intelligence servers, and power modules for new energy vehicles, among other high-heat-flux-density scenarios [12–14]. At present, research on thermal conductive gels primarily focuses on enhancing their thermal conductivity. The main strategies include incorporating nano or micro-scale thermal conductive fillers, such as boron nitride, aluminum oxide, and silicon carbide, as well as developing novel polymer matrices (e.g., modified epoxy resins and silicone-based systems) to optimize the mechanical properties and thermal stability of the materials [15–21]. For thermal conductive gels, practical applications require consideration not only of their intrinsic properties but also of their process compatibility. bonding strength reflects the interfacial reliability between the thermal conductive gel and the chip and can serve as a key mechanical parameter for evaluating processing adaptability [22–24]. It is primarily influenced by processing parameters, including filler ratio, silicone oil viscosity, and wetting time [25]. However, the underlying mechanisms and governing principles by which processing parameters influence the viscosity of thermal conductive gels remain insufficiently understood. In addition, current application evaluations predominantly focus on the intrinsic material properties, which makes it difficult to accurately simulate the influence of thermal conductive gels on device junction temperature and thermal resistance under realistic operating conditions. Consequently, discrepancies often arise between laboratory evaluation results and actual service performance. Therefore, to achieve high performance thermal conductive gels, it is essential to systematically investigate both process optimization strategies and more application-oriented evaluation methods.

In this study, an orthogonal experimental design was employed to systematically investigate the effects of filler ratio, wetting time, and silicone oil viscosity on the bonding strength of thermal conductive gels, aiming to determine the optimal combination of processing parameters that simultaneously ensures high thermal conductivity and excellent process adaptability.

Subsequently, the thermal conductivity and thermal resistance of both commercial thermal conductive gels and the as-prepared gels were characterized using the steady-state heat flow method and the double-interface method, respectively. Using commercial thermal conductive gel as the control, both the intrinsic thermal conductivity and the service thermal resistance were comparatively evaluated. The results demonstrate the superior thermal performance of the self-developed gel, providing valuable guidance for the development and practical application of thermal conductive gels in chip thermal management.

2. Materials and Methods

In this study, vinyl silicone oil (model VS100, Jiangmen U-Bond New Material Co., Ltd., China) was used as the gel matrix, while hydrogen-containing silicone oil (model HS200, Jiangmen U-Bond New Material Co., Ltd., China) served as the crosslinking agent. A mixed filler composed of aluminum powder and zinc oxide (model AZ300, Dongguan Eunow Chemical Co., Ltd., China) was employed as the thermally conductive filler. Alkynol (model BY400, Dongguan Eunow Chemical Co., Ltd., China) was used as the inhibitor, and a platinum complex catalyst (model PT500, Jiangmen U-Bond New Material Co., Ltd., China) was adopted as the curing catalyst.

Gel preparation: Vinyl silicone oil (5-15 wt%), hydrogen-containing silicone oil (1.8 wt%), mixed filler (aluminum powder and zinc oxide, 83-93 wt%), and platinum complex (0.2 wt%) were weighed according to the designed formulation. A DLH-5L power mixer (Foshan Jinyinhe Intelligent Equipment Co., Ltd., China) was employed for the preparation process. Initially, vinyl silicone oil

© 2026 by the author(s). Distributed under a Creative Commons CC BY license.

Preprints.org (www.preprints.org) | NOT PEER-REVIEWED | Posted: 2 March 2026 doi:10.20944/preprints202603.0106.v1

and the mixed filler were blended and stirred at room temperature for 120-180 min to ensure uniform dispersion, followed by standing for 14-18 h. After confirming homogeneous dispersion, the mixture was heated to 130-180 °C under vacuum to remove residual moisture. Subsequently, the system was cooled to room temperature, and hydrogen-containing silicone oil together with alkynol was added. The mixture was further dispersed uniformly and subjected to vacuum treatment. Finally, the platinum complex catalyst was incorporated, and the thermal conductive gel was obtained after thorough dispersion and vacuum defoaming.

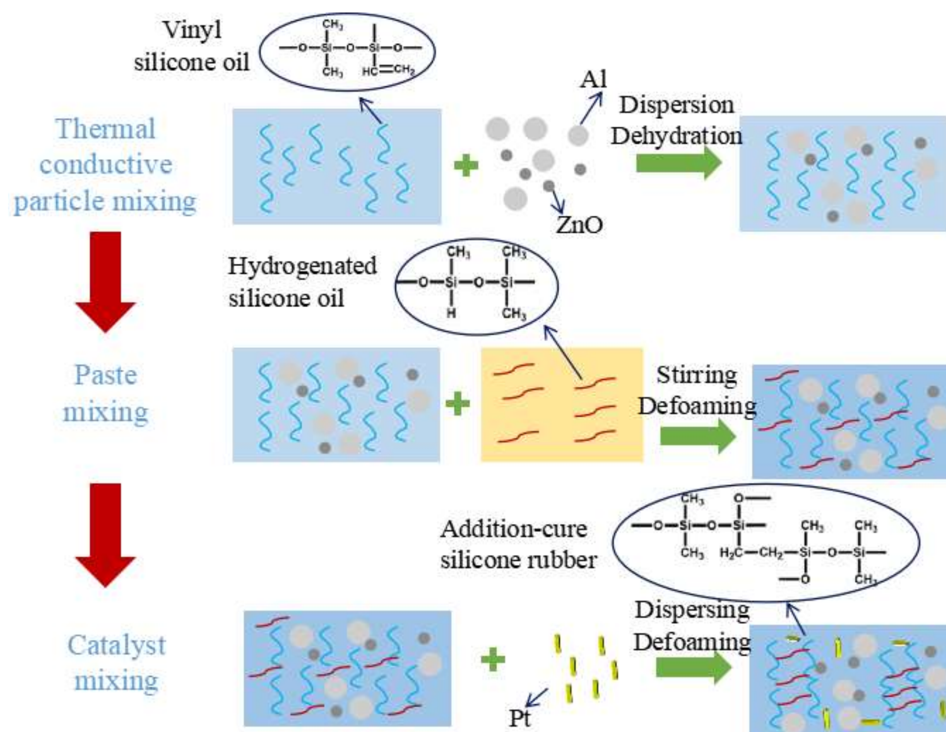

Figure 1. Flow chart of thermal conductive gel preparation.

To evaluate performance at both the material and device levels, a commercial thermal conductive gel (Shin-Etsu, model X23-7772-24, Japan) was employed as the control sample. For clarity, the self-developed thermal conductive gel and the commercial product are here after denoted as thermal conductive gel A and thermal conductive gel B, respectively.

Characterization method: the bonding strength of the thermal conductive gels under different processing parameters was measured using a tensile shear tester (DAGE 4000, Nordson, USA). According to the ASTM D5470-17 (2024) standard, the thermal conductivity was determined using a steady-state heat flow apparatus (LW-9389, Ruiling Instruments, Taiwan, China). Based on the IEC 61189-2-808 international standard, the contact thermal resistance under service conditions was evaluated using a thermal transient tester (Simcenter T3STER SI, Siemens EDA, Hungary). The minimum bond-line thickness (BLT) and the filler morphology of the thermal conductive gels were characterized using an ultra-depth-of-field microscope (DVM6, Leica Microsystems, Germany) and a scanning electron microscope (Apreo 2, Thermo Fisher Scientific, USA), respectively.

3. Results and Discussion

3.1. Process Optimization and Preparation of Thermal Conductive Gel

As shown in Table 1, a three-factor, three-level orthogonal experimental design was established to investigate the effects of filler ratio, silicone oil viscosity, and wetting time on the shear properties of the thermal conductive gel. The independent variables were filler ratio, silicone oil viscosity, and wetting time, while the dependent variable was the bonding strength of the thermal conductive gel

© 2026 by the author(s). Distributed under a Creative Commons CC BY license.

Preprints.org (www.preprints.org) | NOT PEER-REVIEWED | Posted: 2 March 2026 doi:10.20944/preprints202603.0106.v1

[26–28]. Table 1 presents the bonding strength results of nine groups of thermal conductive gels prepared under different processing parameter combinations.

Table 1. Orthogonal test table for the effects of different filler ratios, viscosity of silicone oil, and wetting time on the bonding strength of thermal conductive gels.

Serial number	Filler ratio (%)	Silicone oil viscosity (cP)	Wetting time (h)	bonding strength (MPa)
1	88	600	14	0.147
2	88	645	18	0.135
3	88	568	10	0.124
4	89	600	18	0.142
5	89	645	10	0.130
6	89	568	14	0.129
7	87	600	10	0.105
8	87	645	14	0.113
9	87	568	18	0.107

Range analysis was conducted to evaluate the influence of filler ratio, silicone oil viscosity, and wetting time on the bonding strength of the thermal conductive gel. The range value reflects the degree of variation in the experimental index; a larger range indicates a more significant effect of the corresponding factor on bonding strength. Therefore, the relative importance of the three factors can be ranked according to their range values. The results of the range analysis are presented in Figure 2(d). The calculated ranges for filler ratio, silicone oil viscosity, and wetting time were 0.027 MPa, 0.011 MPa, and 0.010 MPa, respectively. These results indicate that the filler ratio is the most influential factor affecting bonding strength, followed by silicone oil viscosity, while wetting time exhibits the least effect. As shown in Figure 2(a), the bonding strength of the thermal conductive gel initially increases and subsequently decreases with increasing filler ratio. This phenomenon can be primarily attributed to the fact that the bonding strength of the thermal interface material fundamentally depends on the interfacial interactions between the filler particles and the silicone oil matrix. A higher density of contact sites between the filler and the silicone oil enhances mechanical interlocking and interfacial adhesion, thereby improving the overall bonding strength. However, when the filler content is further increased beyond an optimal level, particle agglomeration may occur, leading to non-uniform dispersion and a consequent reduction in effective interfacial adhesion.

As shown in Figure 2(b), silicone oil viscosity governs the degree of molecular chain entanglement and fluidity within the matrix. An increase in viscosity generally corresponds to longer molecular chains, which enhances adsorption and interfacial entanglement with the filler surface, thereby strengthening interfacial cohesion. Nevertheless, excessively high viscosity compromises flowability, hindering the complete wetting of filler particles. This insufficient wetting reduces the effective interfacial contact area between the matrix and filler, ultimately weakening the bonding strength. Compared with the filler, the silicone oil matrix cannot substitute for the mechanical framework established by the filler network. Since the structural integrity and load-bearing capability are predominantly determined by the filler skeleton, the influence of silicone oil viscosity is inherently constrained, resulting in a weaker overall effect than that of the filler ratio.

As shown in Figure 2(c), wetting time exhibits the least influence among the three factors. Its role is primarily associated with the infiltration and wetting process of silicone oil onto the filler surface, which is characterized by a saturation effect. Insufficient wetting (e.g., within 10 h) results in incomplete interfacial infiltration, leading to the formation of interfacial voids and consequently reduced bonding strength. When the wetting time is extended to approximately 14 h, the silicone oil sufficiently envelops the filler particles and effectively fills the interfacial gaps, thereby enhancing interfacial integrity. Further prolonging the wetting time to 18 h does not significantly improve the infiltration behavior or interfacial bonding quality, indicating that the wetting process has reached

© 2026 by the author(s). Distributed under a Creative Commons CC BY license.

Preprints.org (www.preprints.org) | NOT PEER-REVIEWED | Posted: 2 March 2026 doi:10.20944/preprints202603.0106.v1

equilibrium. Based on the range analysis results, the optimal preparation parameters were determined to be a filler ratio of 88 wt%, a silicone oil viscosity of 600 cP, and a wetting time of 14 h. Under these conditions, the bonding strength reached 0.147 MPa.

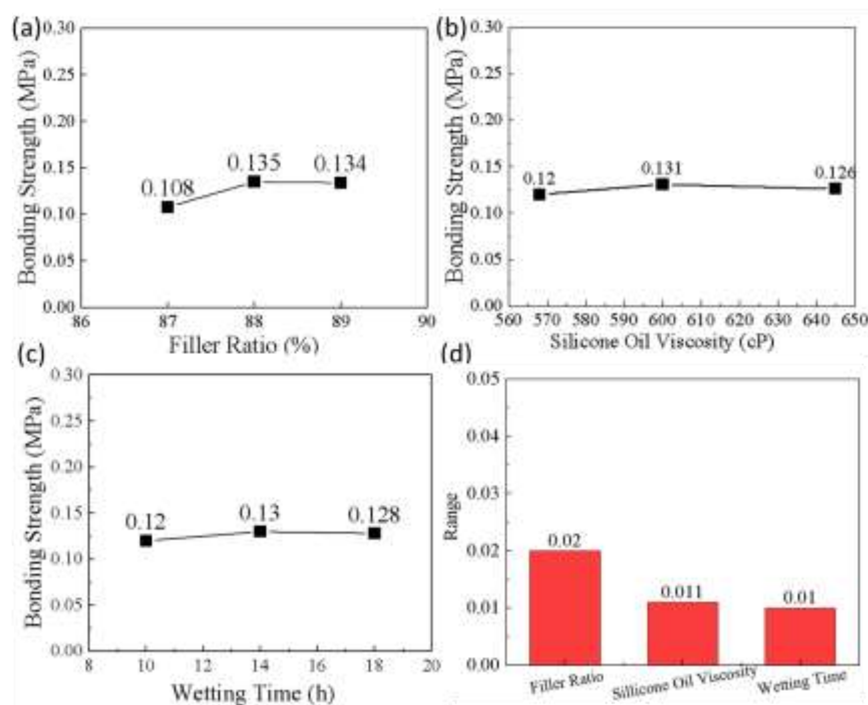

Figure 2. Influence trends and ranges of different factors on the shear strength of thermal conductive gels: (a) Filler ratio, (b) silicone oil viscosity, (c) wetting time, and (d) ranges of the three factors.

3.2. Characterization of Intrinsic Thermal Conductivity of Thermal Conductive Gels

As shown in Figure 3(a), the thermal conductivity of thermal conductive gel A and thermal conductive gel B was measured using a steady-state heat flow apparatus. During the test, the temperature of the hot side was maintained at 50 °C. The gap distance between the hot and cold sides was adjusted to 0.337 mm, 0.221 mm, and 0.107 mm, respectively. Under steady-state conditions, the input power and the temperature at the cold side were recorded for thermal conductivity calculation

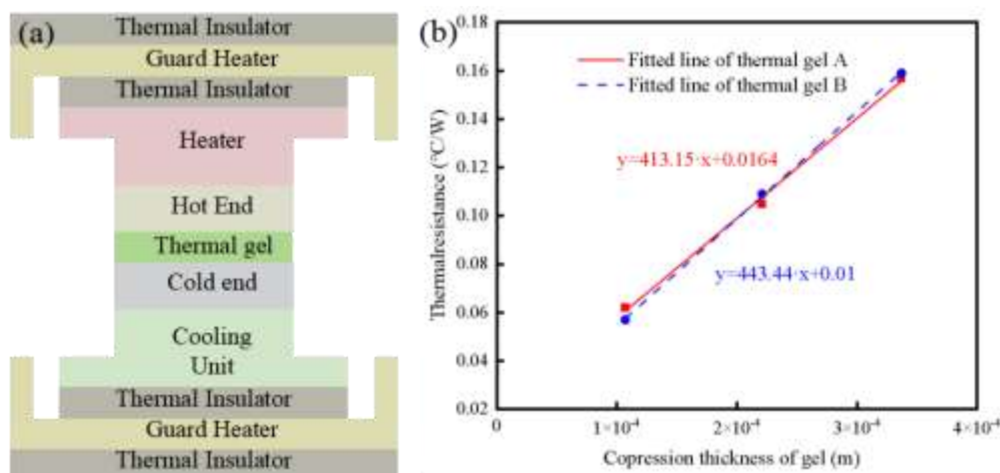

Figure 3. Schematic diagram and test results of the steady-state heat flow measurement for thermal conductive gels: (a) Schematic diagram of steady-state heat flow measurement for thermal conductive gels, (b) Variation of gel thermal resistance with compressed thickness.

© 2026 by the author(s). Distributed under a Creative Commons CC BY license.

Preprints.org (www.preprints.org) | NOT PEER-REVIEWED | Posted: 2 March 2026 doi:10.20944/preprints202603.0106.v1

According to Equation (1), the thermal resistance of the two thermal conductive gels at different compression thicknesses was calculated, and the corresponding results are summarized in Table 2.

$$R = \frac{T_2 - T_1}{P} \tag{1}$$

In Equation (1), R denotes the thermal resistance, T_1 and T_2 represent the temperatures of the hot and cold sides, respectively, and P corresponds to the input power applied to the thermal conductive gel.

Table 2. Temperature of cold end and hot end of the steady-state heat flow device under different compressed thickness.

Gel Type	Heat transfer area (mm)	Compression thickness (mm)	Hot end temperature (°C)	Cold end temperature (°C)	Input power (W)	thermal resistance (°C·W^{-1})
Thermal	6.452	0.337	50	45.45	28.46	0.157
conductive gel	6.452	0.221	50	46.59	30.31	0.105
A	6.452	0.107	50	47.89	33.82	0.062
Thermal	6.452	0.337	50	45.82	28.61	0.159
conductive gel	6.452	0.221	50	47.10	31.22	0.109
B	6.452	0.107	50	48.21	34.36	0.057

As shown in Figure 3(b), the thermal resistance of both thermal conductive gels increases linearly with increasing compression thickness. In the steady-state heat flow measurement, the total thermal resistance of the thermal conductive gel is primarily composed of intrinsic (bulk) thermal resistance and interfacial thermal resistance, as described by Equations (2)-(4) [29,30].

$$R = R1 + R0 \tag{2}$$

$$R1 = d/(\lambda \cdot A) \tag{3}$$

$$R = d/\lambda + R0 \tag{4}$$

In these equations, R_0 and R_1 represent the interfacial thermal resistance and intrinsic (bulk) thermal resistance, respectively; d denotes the sample thickness; λ is the thermal conductivity; and A corresponds to the heat dissipation area. By linearly fitting the thermal resistance values of thermal conductive gels A and B at different thicknesses, the relationships between thermal resistance and thickness were obtained, as expressed in Equations (5) and (6).

$$y = 413.15 \cdot x + 0.0164 \tag{5}$$

$$y = 444.54 \cdot x + 0.0098 \tag{6}$$

From the fitted equations, it can be inferred that the slopes of the two linear plots in Figure 3(b) are positively correlated with the reciprocal of the thermal conductivity of the respective thermal conductive gels. Based on the linear fitting results, the thermal conductivities of thermal conductive gels A and B were calculated to be 3.75 W·m^{-1}·K^{-1} and 3.49 W·m^{-1}·K^{-1}, respectively.

As shown in Figure 4, previous studies by Tong, Yang, and other researchers have reported that the thermal conductivity of most existing thermal conductive gels is primarily distributed within the range of 1-3.5 W·m^{-1}·K^{-1} [31,32]. Therefore, the self-developed thermal conductive gel exhibits a thermal conductivity approximately 7.1% higher than that of the commercial counterpart, demonstrating its superior heat transfer capability.

© 2026 by the author(s). Distributed under a Creative Commons CC BY license.

Preprints.org (www.preprints.org) | NOT PEER-REVIEWED | Posted: 2 March 2026 doi:10.20944/preprints202603.0106.v1

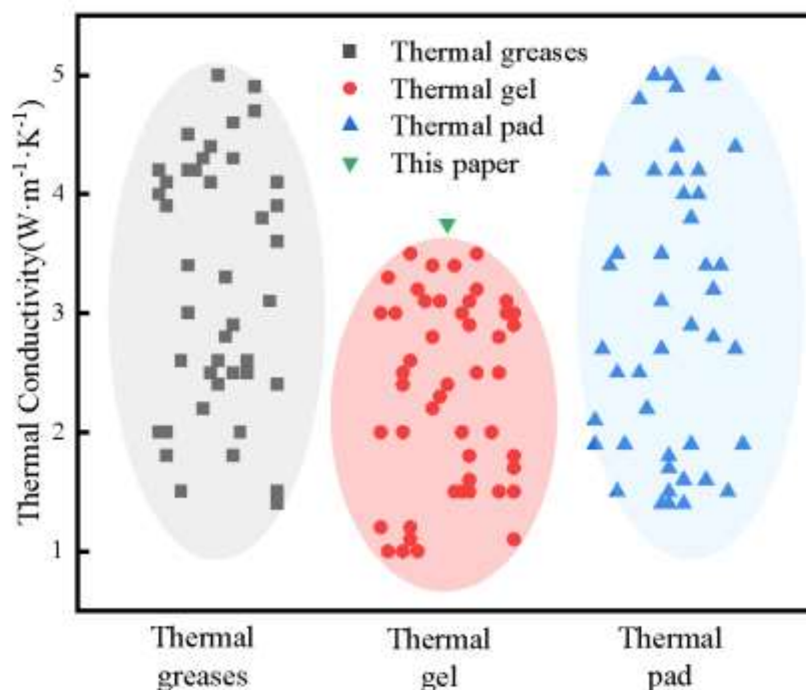

Figure 4. Comparison of thermal conductivity of different types of thermal interface materials.

3.3. Thermal Resistance Test of Thermal Conductive Gel in Service

As shown in Figure 5, the service thermal resistance of the thermal conductive gels was evaluated using the double-interface method in accordance with the IEC 61189-2-208 standard. A SiC diode with a constant power dissipation of 9 W and a bottom heat dissipation area of 1 cm^2 was employed as the heat source. The junction temperature and thermal resistance of the device were recorded sequentially under dry and wet steady-state conditions. As illustrated in Figure 5(c), the junction temperature of the SiC device under dry test conditions was 48.3 °C. After applying thermal conductive gel A and thermal conductive gel B (wet condition), the junction temperatures decreased to 36.6 °C and 37.9 °C, respectively.

For the SiC diode, natural convection from the top surface was considered negligible, and heat dissipation was assumed to occur sequentially through the chip, solder layer, lead frame, thermal conductive gel, and heat sink [33]. As illustrated in Figure 5(b), the actual packaging structure of the SiC diode was modeled using a Cauer thermal network model. In this model, thermal capacitance represents the heat storage capability of each material layer. However, under steady-state heat transfer conditions, the effect of thermal capacitance can be neglected because the heat flow becomes time-independent. Therefore, in the steady state, the Cauer thermal network of the SiC diode simplifies to a series cascade of thermal resistances corresponding to the individual packaging layers [34,35]. Due to the differences in thermal conductivity and thermal capacitance among the constituent materials, distinct thermal resistance-thermal capacitance (R-C) characteristic curves are obtained. Based on the double-interface method and the corresponding transient thermal response curves, the thermal resistance of the thermal conductive gel can be extracted. As shown in Figure 5(d), the service thermal resistances of thermal conductive gel A and thermal conductive gel B were determined to be 0.611 $°C·W^{-1}$ and 0.723 $°C·W^{-1}$, respectively. These results are consistent with the junction temperature analysis of the SiC diode discussed above. The lower thermal resistance of thermal conductive gel A indicates its superior heat dissipation capability compared with thermal conductive gel B.

© 2026 by the author(s). Distributed under a Creative Commons CC BY license.

doi:10.20944/preprints202603.0106.v1

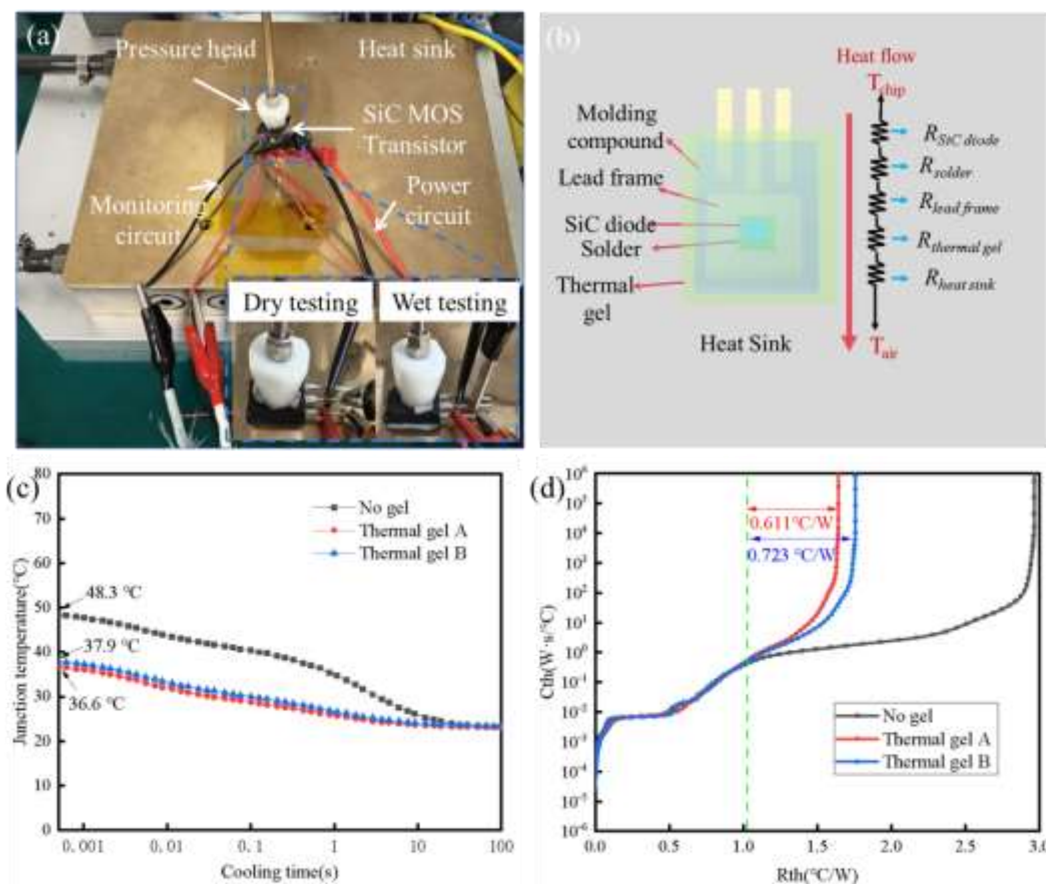

Figure 5. Dual-interface method test setup, thermal resistance network model, and test results for thermal conductive gess: (a) Dual-interface method test setup, (b) thermal resistance network model of the SiC diode, (c) junction temperature of the SiC diode, (d) in-service thermal resistance of the thermal conductive gels.

3.4. Analysis of Heat Transfer Mechanism of Thermal Conductive Gel

To elucidate the origin of the difference in heat dissipation performance between thermal conductive gel A and thermal conductive gel B, the minimum bond-line thickness (BLT) of the two gels was characterized using an ultra-depth-of-field microscope. The corresponding results are presented in Figure 6(a) and (b). The BLT values of thermal conductive gel A and thermal conductive gel B were measured to be 15.9 μm and 17.9 μm, respectively. According to Equation (3), the intrinsic (bulk) thermal resistances of thermal conductive gel A and thermal conductive gel B were calculated to be 0.042 $°C·W^{-1}$ and 0.051 $°C·W^{-1}$, respectively. According to Equation (4), the interfacial thermal resistances of thermal conductive gel A and thermal conductive gel B were calculated to be 0.569 $°C·W^{-1}$ and 0.672 $°C·W^{-1}$, respectively. In other words, thermal conductive gel A exhibits lower intrinsic (bulk) thermal resistance as well as lower interfacial thermal resistance compared with thermal conductive gel B.

To further elucidate the origin of the difference in heat dissipation performance between the two thermal conductive gels, the micro-structural morphology of the fillers was analyzed after removing the organic matrix via thermal decomposition. As shown in Figure 6(a) and (b), the thermal conductive fillers in both gels consist of large-sized Al particles and small-sized ZnO particles, forming a bimodal particle size distribution. Compared with thermal conductive gel B, the Al particles in thermal conductive gel A exhibit a smaller average diameter (14.16 μm) and are more uniformly coated by ZnO particles, resulting in a more homogeneous filler distribution. Considering that the thermal conductivity of vinyl silicone oil is only 0.2 $W·m^{-1}·K^{-1}$, whereas that of Al and ZnO are 247 $W·m^{-1}·K^{-1}$ and 5 $W·m^{-1}·K^{-1}$, respectively [36], heat conduction within the thermal conductive gels is predominantly governed by the thermally conductive filler network rather than the polymer

© 2026 by the author(s). Distributed under a Creative Commons CC BY license.

matrix. As shown in Figure 6(c) and (d), the reduced particle size of Al shortens the effective heat transfer distance and facilitates the formation of more continuous thermal conduction pathways. Consequently, the minimum BLT of the thermal conductive gel can be further reduced, which contributes to the overall decrease in intrinsic thermal resistance.

Moreover, the reduced particle size of Al increases the effective contact area between the thermal conductive gel and both the device surface and the heat sink. This enlarged interfacial contact area enhances phonon and electron coupling across the interface, thereby optimizing the heat dissipation pathway and effectively reducing the interfacial thermal resistance of the thermal conductive gel. In addition, the uniform dispersion of fine ZnO particles around the Al particles enables efficient filling of the interstitial voids between adjacent Al particles. This structural arrangement increases the packing density of the filler network and promotes the formation of more continuous thermal conduction pathways. As a result, the intrinsic (bulk) thermal resistance of the thermal conductive gel is further reduced.

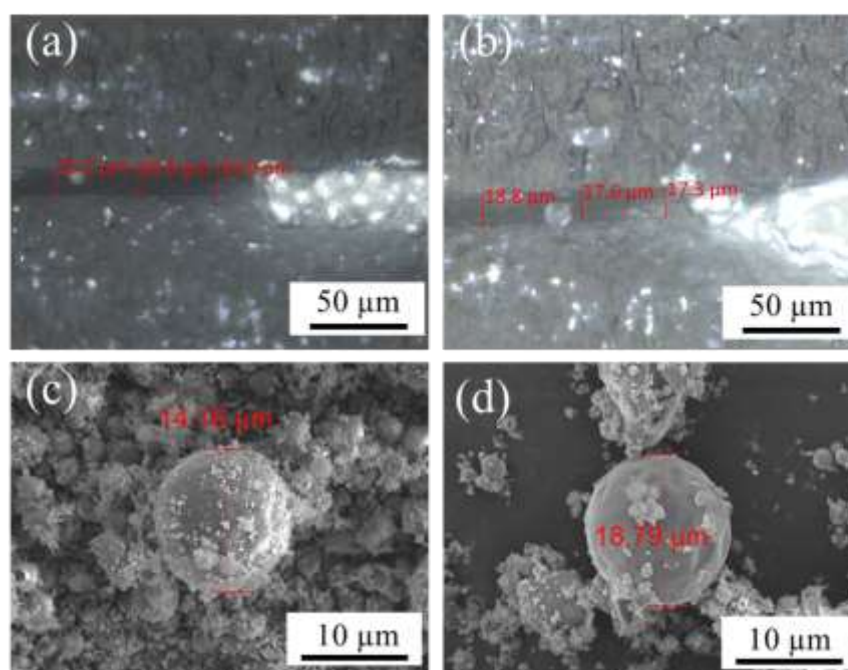

Figure 6. SEM images of the thermal conductive gel A (a), and B (b), (c, d) the diameters of Al particles in the thermal conductive gels A and B.

4. Conclusions

In summary, the rheological and mechanical properties of the thermal conductive gel can be effectively regulated by adjusting the filler ratio, silicone oil viscosity, and wetting time. Among these parameters, the filler ratio exhibits the most significant influence on bonding strength, followed by silicone oil viscosity, while wetting time shows the weakest effect. Under the optimized preparation conditions (filler ratio of 88%, silicone oil viscosity of 600 cP, and wetting time of 14 h), the bonding strength of the thermal conductive gel reached 0.147 MPa.

The thermal conductivity and thermal resistance of the self-developed thermal conductive gel were systematically characterized using the steady-state heat flow method and the double-interface method, respectively. The thermal conductivity and overall thermal resistance were determined to be 3.75 $W{\cdot}m^{-1}{\cdot}K^{-1}$ and 0.611 $°C{\cdot}W^{-1}$, respectively, both superior to those of the commercial reference gel. These results demonstrate the enhanced heat dissipation capability and promising application potential of the developed material in thermal management systems.

The filler architecture plays a decisive role in determining the thermal and mechanical performance of the thermal conductive gel. Large-sized Al particles predominantly influence BLT

© 2026 by the author(s). Distributed under a Creative Commons CC BY license.

Preprints.org (www.preprints.org) | NOT PEER-REVIEWED | Posted: 2 March 2026 doi:10.20944/preprints202603.0106.v1

and interfacial thermal resistance, while fine ZnO particles effectively fill the interstitial voids between adjacent Al particles, promoting the formation of continuous thermal conduction pathways and reducing intrinsic thermal resistance. The synergistic effect of the bimodal filler structure contributes to the overall improvement in heat dissipation performance.

Informed Consent Statement: This research does not involve any studies with human participants or animals conducted by the authors.

Data Availability Statement: The data supporting the findings of this study are available from the corresponding author upon reasonable request.

Acknowledgments: The authors gratefully acknowledge the financial support provided by the Key-Area Research and Development Program of Guangdong Province (Grant Nos. 2024B0101080002 and 2024B0101120004).

Conflicts of Interest: The authors declare that they have no known competing financial interests or personal relationships that could have influenced the work reported in this paper.

References

1. Feng, C.; Yang, L.; Yang, J.; et al. Recent advances in polymer-based thermal interface materials for thermal management: A mini-review. *Compos. Commun.* **2020**, *22*, 100528.
2. Rahru, R.; Faiz, M.; Halim, A.; et al. A review of thermal interface material fabrication method toward enhancing heat dissipation. *Energy Res.* **2021**, 45, 3548–3568.
3. Dhumal, A.R.; Kulkarni, A.P.; Ambhore, N.H. A comprehensive review on thermal management of electronic devices. *J. Eng. Appl. Sci.* **2023**, *70*, 140.
4. Chakarvarti, S.K.; Gehlawat, D.; Manocha, A. Thermal interface materials for thermal management of microelectronic devices: A review. *J. Therm. Anal. Calorim.* **2025**, *150*, 8847–8860.
5. Cheng, Z.; Han, Y.; Zhang, X. Investigation of the thermal conductance of MEMS contact switches. *Micromachines* **2025**, *16*, 120.
6. Susani, L.B.; Coda, F.; Santomauro, M. Reliability of thermal interface materials in combined mechanical and thermal stress. In Proceedings of the 2023 22nd IEEE Intersociety Conference on Thermal and Thermomechanical Phenomena in Electronic Systems (ITherm), **2023**; pp. 1–7.
7. Asif, M.; Husain, S.; Rehman, S.; et al. Experimental studies on selected thermal interface materials. *Therm. Sci.* **2024**, *28*, 2857–2866.
8. Pedram, M.; Nazarian, S. Thermal modeling, analysis, and management in VLSI circuits: Principles and methods. *Proc. IEEE* **2006**, *94*, 1487–1501.
9. Singh, P.K.; Singh, A.K.; Singh, V.K. Impact of the pump-out-effect on the thermal long-term behaviour of power electronic modules. *Microelectron. Reliab.* **2024**, *155*, 115362.
10. Lewis, J.S.; Perrier, T.; Barani, Z.; Kargar, F.; Balandin, A.A. Thermal interface materials with graphene fillers: Review of the state of the art and outlook for future applications. *Nanotechnol.* **2021**, *32*, 142003.
11. Yang, W.; Kim, J.; Lee, H. Improving the thermal conductivity of an epoxy composite with chemically boron nitride-grafted carbon fiber. *Compos. B Eng.* **2024**, *268*, 111089.
12. Sun, Y.; Ma, Q.; Liang, T.; et al. Optimization of effective thermal conductivity of thermal interface materials based on the genetic algorithm-driven random thermal network model. *ACS Appl. Mater. Interfaces* **2021**, *13*, 45050–45058.
13. Zhang, M.; Wang, Y.; Liu, Z. Application of power battery under thermal conductive silica gel plate in new energy vehicles. *Sci. Rep.* **2024**, *14*, 312.
14. Burger, N.; Laachachi, A.; Ferriol, M.; et al. Review of thermal conductivity in composites: Mechanisms, parameters and theory. *Prog. Polym. Sci.* **2016**, *61*, 1–28.
15. Yang, X.; Zhang, X.; Zhang, T.; et al. Modeling and optimization of thermal interface materials featuring horizontally oriented fillers by flow-field driven strategy. *Compos. Part A* **2025**, *198*, 109157–109169.
16. Leung, S.N. Thermally conductive polymer composites and nanocomposites: Processing structure property relationships. *Compos. Part B* **2018**, *150*, 78–92.

© 2026 by the author(s). Distributed under a Creative Commons CC BY license.

Preprints.org (www.preprints.org) | NOT PEER-REVIEWED | Posted: 2 March 2026
doi:10.20944/preprints202603.0106.v1

17. Zhang, C.; Liu, J.; Sun, R.; et al. Effects of in situ modification of aluminum fillers on the rheological properties and thermal resistance of gel thermal interface materials. *IEEE Trans. Compon. Packag. Manuf. Technol.* **2022**, *12*, 1302–1310.
18. Tu, Y.; Liu, B.; Yao, G.; et al. A review of advanced thermal interface materials with oriented structures for electronic devices. *Electronics* **2024**, *13*, 4287–4314.
19. Wang, Z.; Li, J.; Zhang, X. Significantly enhancing the through-plane thermal conductivity of epoxy dielectrics by constructing aramid nanofiber/boron nitride three-dimensional interconnected framework. *AIP Adv.* **2024**, *14*, 075332.
20. Kim, Y.; Choi, H.; Park, S. Fabrication and characterization of Al_2O_3-siloxane composite thermal pads for thermal interface materials. *Polymers* **2024**, *16*, 543.
21. Zhang, X.; Liu, Y.; Wu, Z. Promoting thermal conductivity of alumina-based composite materials by systematically incorporating modified graphene oxide. *J. Compos. Sci.* **2024**, *8*, 189.
22. Shinde, S.; Sampath, S. A critical analysis of the tensile adhesion test for thermally sprayed coatings. *J. Therm. Spray Technol.* **2022**, *31*, 2247–2279.
23. Wang, Y.; Li, X.; Liu, Z.; et al. A novel modeling and analysis of mechanical properties of single-component thermal conductive silica gel. *Sci. Rep.* **2025**, *15*, 15163.
24. Uddin, M.A.; Alam, M.O.; Chan, Y.C.; Chan, H.P. Adhesion strength and contact resistance of flip chip on flex packages—effect of curing degree of anisotropic conductive film. *Microelectron. Reliab.* **2004**, *44*, 505–514.
25. Yap, T.F.; et al. Understanding silicone elastomer curing and adhesion for stronger soft devices. *Sci. Adv.* **2025**, *11*, 2681.
26. Kumar, A.; Singh, S.; Kumar, R. Optimizing thermal conductivity in 3D-printed composites via Taguchi parameter analysis. *Int. J. Adv. Manuf. Technol.* **2025**, *130*, 2451–2463.
27. Sazali, S.B.; Hassan, H.B.; Yusof, N.; Husaini, Y.; Aziz, A.B.A.; Yaakub, T.N.B.T. Optimization of design parameters using Taguchi method for thermal stress analysis in a 3D IC. *In Proceedings of the 2024 IEEE 14th Symposium on Computer Applications & Industrial Electronics (ISCAIE)*, **2024**; pp. 1–4.
28. Jia, X. The optimization of extrusion process parameters utilizing the Taguchi method. *Int. J. Front. Eng. Technol.* **2024**, *6*, 109–114.
29. Zhang, C.; Ren, L.; Zeng, X.; et al. Effects of rheological properties on the thermal resistance of gel thermal interface materials. *In Proceedings of the 23rd International Conference on Electronic Packaging Technology (ICEPT)*, **2022**.
30. Prasher, R.S.; Matayabas, J.C.; et al. Thermal contact resistance of cured gel polymeric thermal interface material. *IEEE Trans. Compon. Packag. Technol.* **2004**, *27*, 702–709.
31. Tong, X. Advanced Materials for Thermal Management of Electronic Packaging; *Springer:* **2011**.
32. Yang, J.; Tang, L.; Bao, R.; et al. Largely enhanced thermal conductivity of poly(ethylene glycol)/boron nitride composite phase change materials for solar-thermal-electric energy conversion and storage with very low content of graphene nanoplatelets. *Chem. Eng. J.* **2017**, *315*, 481–490.
33. Zhang, B.; Lu, X.; Feng, H.; Wang, Y.; Liu, Y.; Mei, Y.-H. Self-oxygenation silver paste for SiC power modules with high thermal dissipation reliability. *J. Alloys Compd.* **2025**, *1038*, 182720.
34. Alavi, O.; Abdollah, M.; Hooshmand Viki, A. Assessment of thermal network models for estimating IGBT junction temperature of a buck converter. *In Proceedings of the 2017 8th Power Electronics, Drive Systems & Technologies Conference (PEDSTC)*, **2017**; pp. 102–107.
35. Lan, X.; Zhao, N. Development of a steady state electrothermal cosimulation model of SiC power modules. Int. J. *Heat Mass Transf.* **2024**, *266*, 125460.
36. Chung, D.D.L. Materials for thermal conduction. *Appl. Therm. Eng.* **2001**, *21*, 1593–1605.

Disclaimer/Publisher's Note: The statements, opinions and data contained in all publications are solely those of the individual author(s) and contributor(s) and not of MDPI and/or the editor(s). MDPI and/or the editor(s) disclaim responsibility for any injury to people or property resulting from any ideas, methods, instructions or products referred to in the content.

© 2026 by the author(s). Distributed under a Creative Commons CC BY license.